Journal of Biomechanics 152 (2023) 111558

Contents lists available at ScienceDirect

Journal of Biomechanics

journal homepage: www.elsevier.com/locate/jbiomech

Supersonic shear wave elastography of human tendons is associated with *in vivo* tendon stiffness over small strains

Tiziana Mifsud [a,e], Panagiotis Chatzistergos [b,*], Constantinos Maganaris [c], Nachiappan Chockalingam [a,b], Nat Padhiar [d], Kirill Micallef Stafrace [e], Alfred Gatt [a,b]

[a] Faculty of Health Sciences, University of Malta, Msida, Malta
[b] Centre for Biomechanics and Rehabilitation Technologies, Staffordshire University, Stoke-on-Trent, United Kingdom
[c] John Moores University, School of Sport and Exercise Sciences, Liverpool, United Kingdom
[d] Centre for Sports & Exercise Medicine, Queen Mary University of London, United Kingdom
[e] Department of Orthopaedics, Trauma and Sports Medicine, Mater Dei Hospital, Malta

ARTICLE INFO

Keywords:
Ultrasound Imaging
Elasticity Imaging Techniques
Achilles Tendon
Validity of results
Mechanical Stress

ABSTRACT

Supersonic shear wave (SW) elastography has emerged as a useful imaging modality offering researchers and clinicians a fast, non-invasive, quantitative assessment of tendon biomechanics. However, the exact relationship between SW speed and *in vivo* tendon stiffness is not intuitively obvious and needs to be verified. This study aimed to explore the validity of supersonic SW elastography against a gold standard method to measure the Achilles tendon's *in vivo* tensile stiffness by combining conventional ultrasound imaging with dynamometry. Twelve healthy participants performed maximal voluntary isometric plantarflexion contractions (MVC) on a dynamometer with simultaneous ultrasonographic recording of the medial gastrocnemius musculotendinous junction for dynamometry-based measurement of stiffness. The tendon's force–elongation relationship and stress–strain behaviour were assessed. Tendon stiffness at different levels of tension was calculated as the slope of the stress–strain graph. SW speed was measured at the midportion of the free tendon and tendon Young's modulus was estimated. A correlation analysis between the two techniques revealed a statistically significant correlation for small strains ($r(10) = 0.604$, $p = .038$). SW-based assessments of *in vivo* tendon stiffness were not correlated to the gold standard method for strains in the tendon>10 % of the maximum strain during MVC. The absolute values of SW-based Young's modulus estimations were approximately-three orders of magnitude lower than dynamometry-based measurements. Supersonic SW elastography should be only used to assess SW speed for the detection and study of differences between tissue regions, differences between people or groups of people or changes over time in tendon initial stiffness (i.e., stiffness for small strains).

1. Introduction

Supersonic shear wave (SW) elastography has emerged as a useful imaging modality offering researchers and clinicians a fast, non-invasive, quantitative assessment of musculoskeletal biomechanics and soft tissue injury (Chatzistergos & Chockalingam, 2022). Supersonic SW elastography uses acoustic radiation force to generate SWs in the imaged tissue and to measure their propagation speed. In linearly elastic, homogenous and isotropic materials, SW speed can be directly used to calculate the material's Young's modulus (E) as $E = 3\rho C^2$ (equation 1) (Sarvazyan et al., 2013), where C is the SW propagation speed and ρ is the imaged tissue density which is typically assumed to be that of water ($\rho \approx 1000\ kg/m^3$) (Bercoff et al., 2004; Widman et al., 2015). However, since none of the aforementioned conditions are met for biological tissues, the exact relationship between SW speed and tissue stiffness is not intuitively obvious and needs to be verified on a tissue-specific basis.

In the case of tendons, supersonic SW elastography has been used to assess regional differences in material properties (DeWall et al., 2014), to study the effect of ageing (Slane & Thelen, 2015; Slane et al., 2017), loading (Payne et al., 2018b), injury (Crawford et al., 2022) and rehabilitation (Dirrichs et al., 2016). Even though supersonic SW elastography can shed light on aspects of *in vivo* tendon biomechanics that cannot be studied using other more conventional methods, to the authors' knowledge, its validity has only been tested on *ex vivo* tendons

* Corresponding author.
E-mail address: Panagiotis.chatzistergos@staffs.ac.uk (P. Chatzistergos).

https://doi.org/10.1016/j.jbiomech.2023.111558
Accepted 22 March 2023
Available online 27 March 2023

(Haen et al., 2017). *Ex vivo* testing can never truly simulate *in vivo* loading conditions (Maganaris et al., 2017) as the tendons change their mechanical properties depending on the preservation and embalming methods used (Gatt et al., 2021; Liao et al., 2015) and the amount of dehydration during mechanical testing (Verstraete et al., 2015). Thus relying on *ex vivo* testing for validation might give misleading results. For this reason a direct comparison between supersonic SW elastography and *in vivo* measurements of tissue stiffness is needed before supersonic SW elastography can be confidently used to study *in vivo* tendon biomechanics.

The existing gold standard method to assess *in vivo* human tendon biomechanics assumes that the tendon is a single uniform spring and combines conventional ultrasound imaging with dynamometry to measure its tensile stiffness. The tendon's force–elongation relationship is measured during voluntary maximal contraction (MVC) (Maganaris & Paul, 1999). Combined with sonographic measurements of tendon dimensions, this measurement of force and elongation is used to estimate the tendon's stress–strain behaviour and Young's modulus. To improve the accuracy of these estimates, an actual measurement of the tendon's moment arm (Maganaris, 2004) and accounting for the effect of muscle antagonistic co-activation (Maganaris et al., 1998) are also necessary. Overall, the dynamometry-based assessment of tendon mechanical properties is significantly more complicated and time-consuming than SW elastography, and although it offers a complete assessment of the visco-elastic behaviour of the tendon under clinically relevant tensile loading, it is not capable of measuring regional differences in tendon stiffness.

SW elastography with its capacity to detect regional differences in tissue properties appears the ideal candidate to fill this gap. In existing validated applications of SW elastography, patterns of increased regional SW speed are able to detect lesions and differentiate between benign and malignant skin lesions (Botar-Jid et al., 2016). The exploration of the physical meaning of SW speed in the heel pad has shown that supersonic SW elastography enables the assessment of differences or changes in initial soft tissue stiffness; namely stiffness for very small strains (Chatzistergos et al., 2018). However, in the case of tendons, the exact meaning of SW speed values remains unclear. Understanding the validity of SW speed is crucial to decide whether/when to use SW elastography and to inform accurate interpretation of its results. A relevant exploration of the physical meaning of SW speed is not available in the literature for tendons.

In the context of the present study, we take measurements in the human Achilles tendon to test the validity of SW speed against a gold standard, dynamometry-based method and to compare and understand the absolute values of SW based Young's modulus.

2. Method

2.1. Participants

A cohort of 12 healthy participants (male/female: 8/4, age: 41y ± 11y, body mass: 74 kg ± 19 kg and height:1.76 m ± 0.10 m) were included. Volunteers had no recent history of lower limb injury or surgery, no pre-existing neuromuscular disorder or musculoskeletal problems. Achilles tendon health was determined through a clinical examination performed by a licensed podiatrist. Only the right leg was tested, which led to the assessment of 9 dominant and 3 non-dominant legs. Leg dominance was determined by the subject-reported preferred kicking leg (Bjornaraa & Di Fabio, 2011; Chiu et al., 2016).

The study protocol for this cross-sectional observational study was approved by Staffordshire University's ethics committee (ethical approval reference number: SU_21_160). All subjects provided written informed consent prior to participation. All data collection was done in a single session of one hour at Staffordshire University. The order of testing was kept the same for every-one as described below.

2.2. Dynamometry-based measurement of stiffness

2.2.1. Measurement of tendon dimensions and moment arm quantification

The medial gastrocnemius musculotendinous junction (MTJ) (Fig. 1a) and the osteotendinous junction of the Achilles tendon were imaged in both the transverse and longitudinal planes and marked on the skin. The MTJ was identified as the point where the deep and superficial gastrocnemius aponeuroses merged with the Achilles tendon. The osteotendinous junction was identified as the most proximal part of the tendon attaching to the calcaneum (Fig. 1c). The distance between the two points was measured with a measuring tape and represented the original length of the whole tendon (Fig. 1d). The soleus tendon junction was then identified (Fig. 1b), marked and measured from the osteotendinous junction of the Achilles tendon's mark, representing the length of the free tendon (Fig. 1d). Tendon cross-sectional area (CSA) of the free tendon was measured in a transverse plane 5 cm proximal to the osteotendinous junction of Achilles tendon (Stenroth et al., 2016). The above measurements were completed with the participant lying prone.

The moment arm of the Achilles tendon was quantified for every individual in the upright position as the perpendicular distance from the centre of rotation of the ankle to the tendon's line of action (Fig. 2). The ankle's centre of rotation was approximated as the centre of the lateral malleolus, assessed by palpation over the skin (Scholz et al., 2008). The tendon's line of action was approximated by a line connecting the centres of its cross-section at 5 cm and 10 cm from the calcaneal insertion (Scholz et al., 2008; Zhao et al., 2009) (Fig. 2a). To complete this measurement the tendon's cross-section was imaged again at 5 and 10 cm from the calcaneal insertion in the transverse plane parallel to the ground (Fig. 2b,c). These images were used to measure the distance between the skin and the centre of the tendon's cross-section. The skin to the centre of tendon distances were transferred onto a lateral photograph of the participant's foot to enable the definition of the tendon's line of action and the direct measurement of its moment arm (Fig. 2a).

All ultrasound imaging was performed using the Aixplorer 4

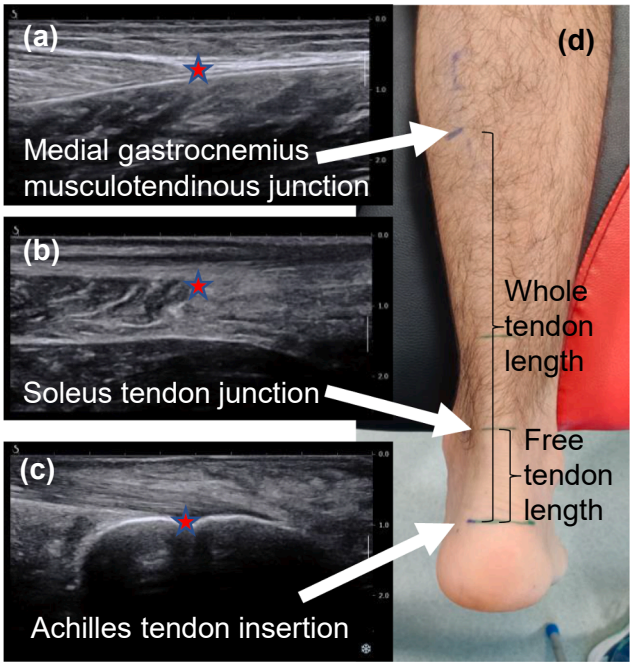

Fig. 1. Longitudinal ultrasound images of the medial gastrocnemius musculotendinous junction (a), soleus tendon junction (b), and Achilles tendon insertion (c) respectively. (d) Markings on the skin of the medial gastrocnemius musculotendinous junction, soleus tendon junction, and Achilles tendon insertion for the measurement of the free tendon length and original length of the whole tendon.

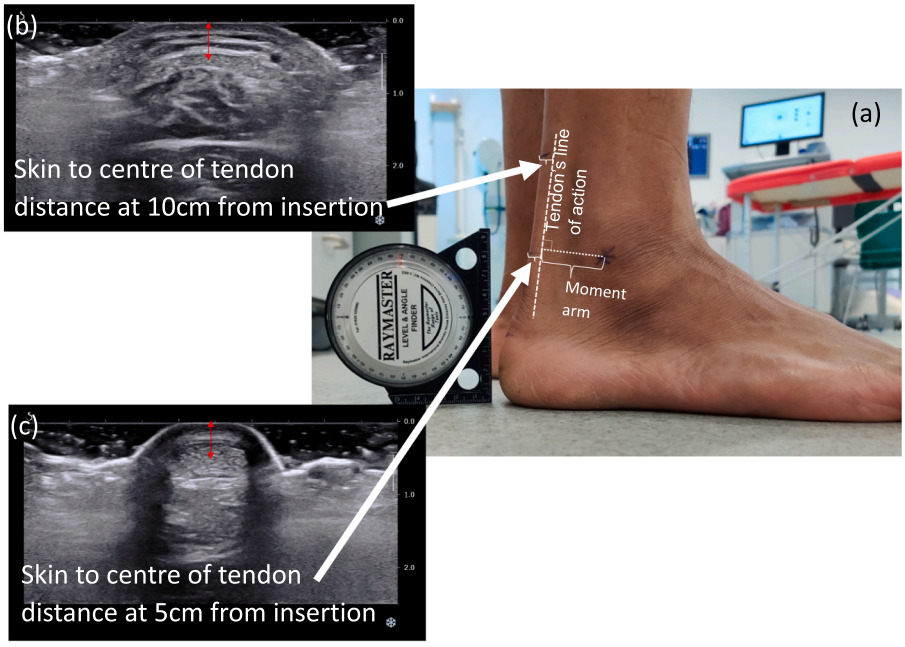

Fig. 2. (a) The lateral photograph used for moment arm calculations. Markings on the skin for the inferior tip of lateral malleolus and on the Achilles tendon at 5 cm and 10 cm from insertion are also visible. The lines drawn on the photograph correspond to the distance between skin and the centre of the tendon, the resulted tendon's line of action and moment arm. (b,c) Transverse ultrasound image at 5 cm and 10 cm respectively proximal to the calcaneal insertion.

MultiWave™ Ultrafast™ Imaging and ShearWave™ Elastography Ultrasound System (Supersonic Imaging, Aix-en-Provence, France) and a linear 4–15 MHz transducer (SuperLinear™ SL15-4).

2.2.2. Calculation of stress–strain behaviour

A warm-up of 5 min was performed on a stationary bike. The participant was then seated on the chair of a dynamometer (Biodex™ Medical System 4 Dynamometer) with their right knee fully extended (supported to avoid hyperextension) and their ankle at 90° relative to the leg (Fig. 3a). Straps were used to secure the subjects in place during MVC. Heel movement was minimised during the contraction by firmly securing the foot in the dynamometer with inextensible tape around the midfoot and ankle. The ankle joint axis passing from the medial and lateral malleolus was visually aligned with the axis of rotation of the dynamometer. The ultrasound probe was securely attached to the lower leg perpendicular to the skin with a customized probe holder, clearly visualising the MTJ in a sagittal plane (Fig. 3b). An ultrasound-absorbing marker was fixed on the skin within the transducer's field of view to mitigate the risk of inaccurate tendon elongation measurements due to heel movement during MVC (Arampatzis et al., 2005; Maganaris, 2005).

Prior to testing, five forceful ankle plantar flexion contractions (five seconds isometric ramped contraction and one-minute rest) were performed for familiarisation and preconditioning of the triceps surae muscle–tendon complex (Maganaris, 2003). Following this, the subjects performed one isometric contraction by gradually increasing the ankle plantar flexion moment over a five second period from a relaxed state to maximal effort. This was repeated twice, with a two-minute rest in between. Verbal encouragement was provided during each trial. Synchronisation of the data recorded by the dynamometer and the ultrasound unit was achieved by simultaneously pushing the dynamometer plate and the probe to produce "events" clearly visible in both systems. Six synchronisation events were produced in total (three before and three after each MVC).

The linear displacement of the tendon during each MVC was recorded with cine-loop ultrasound recordings. Measurements of displacement were taken after the end of all testinghttps://www.kinovea.org/help/en/index.html relative to the ultrasound absorbing marker.

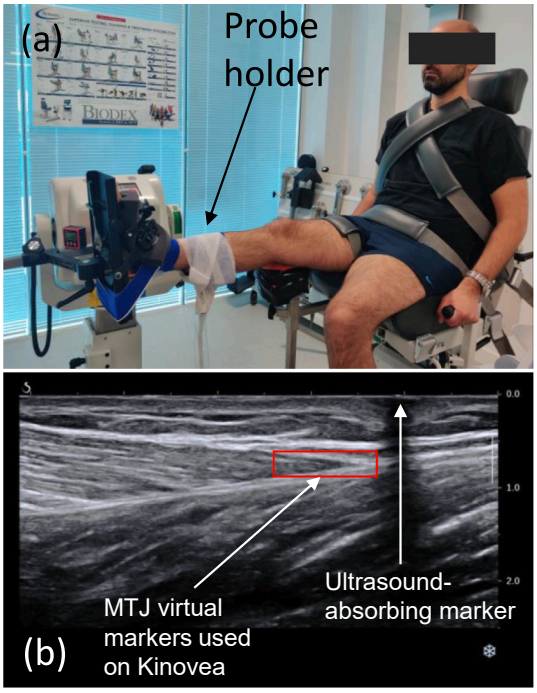

Fig. 3. (a) The testing set up for MVC recording. (b) An image of the medial gastrocnemius musculotendinous junction (MTJ) used for the measurement of tendon elongation. Virtual markers for the tracking of tendon deformation were placed within the marked rectangular area (MTJ virtual markers used on Kinovea). The ultrasound-absorbing marker are also indicated on the figure.

More specifically three virtual markers were placed as close as possible to the MTJ (Arampatzis et al., 2005) and tracked in consecutive frames using Kinovea v0.9.5 (https://www.kinovea.org/help/en/index.html) software (Fig. 3b). The average relative displacement of these three markers was regarded as the estimated displacement of the MTJ.

Achilles tendon force was calculated by dividing the ankle joint

moment by the tendon's moment arm. Tendon stress was obtained by dividing the calculated tendon force over its CSA. The CSA was measured at 5 cm to the insertion of the tendon (Stenroth et al., 2016). Finally, strain was determined by dividing the Achilles tendon's elongation by its resting length to produce a stress–strain graph. Tendon stiffness at different levels of tension was calculated as the slope of this stress–strain graph. To this end, a 6th order polynomial was fitted to the stress–strain data between 0 % and 80 % of maximum elongation. The slope was then algebraically calculated for 10 % to 70 % of the tendon's maximum elongation during MVC in increments of 10 %.

2.2.3. Measurement of antagonist muscle activity

Antagonistic coactivation of the tibialis anterior muscle was captured using electromyography (EMG) (Delsys, Trigno sensors) during the plantarflexion MVCs (Bojsen-Møller et al., 2004). To this end, the electrode was positioned according to the SENIAM guidelines (Merletti, 2000) and the skin was prepared in accordance with European Recommendations for Surface Electromyography (Hermens et al., 1999). In addition to the plantaflexion MVCs, three maximal isometric dorsiflexion MVCs were also performed. For the analysis, a 2nd order Butterworth filter of 20–100 Hz was applied (De Luca et al., 2010) and EMG signals obtained during contractions were full-wave rectified, integrated and root mean square calculated. From the tibialis anterior EMG – dorsiflexion relationship, the antagonistic moment of the dorsiflexors during the plantaflexion MVC's was calculated and accounted for in the calculation of the moment produced by the plantarflexors only (Maganaris et al., 1998), which was then used for further analysis and quantification of forces and stresses.

2.3. Supersonic SW elastography

After finishing the dynamometry-based measurements, the preconditioning five plantarflexion contractions on the dynamometer were repeated for standardisation purposes before taking SW speed measurements. Since regional differences are present along the length of the Achilles tendon (DeWall et al., 2014), all measurements were taken in the middle part of the free tendon (Morgan et al., 2018) while seated on the dynamometer with the ankle in 10° of plantar flexion (Payne et al., 2018a). The participants were asked to completely relax their leg and foot muscles during measurements. A generous amount of coupling gel was used to enable imaging of the Achilles tendon without applying any pressure. More specifically, during imaging, the ultrasound probe was placed along the longitudinal axis of the tendon (Fig. 4). When a clear B-mode image of the tendon was observed, SW elastography was activated. During SW imaging, the upper limit of the colour contour of the elastogram was adjusted to blind the examiner to specific values of SW speed. The transducer was held still for ≈10 s to allow for the elastogram to stabilise before saving a single elastography image (Chatzistergos et al., 2018). The entire imaging process was repeated three times.

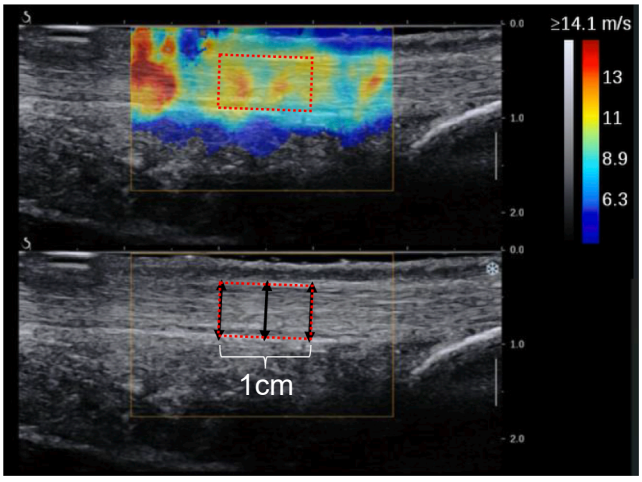

Fig. 4. SW elastography (top) and conventional B-mode imaging (bottom) of the Achilles tendon. The central part of the free tendon is imaged in a longitudinal plane. The locations where thickness was measured (arrows) and the area for which SW speed was calculated (dotted box) are also indicated.

During data extraction, thickness and SW speed were measured for a central 1 cm of the tendon (Fig. 4). More specifically, thickness at the edges and centre of this region of interest (ROI) was measured first (Fig. 4). The arrows that were used to measure thickness were then used as guides to draw a rectangular selection area for the measurement of SW speed (free-form selection). For each image SW speed was averaged within this ROI and the final SW speed measurement was calculated as the average of the three recordings. SW-based Achilles tendon Young's modulus (E) was calculated using equation 1 (Bercoff et al., 2004; Widman et al., 2015).

2.4. Statistical analysis

All statistical tests were performed using SPSS v28 (IBM, Chicago, IL, USA) with the level of significance set at $\alpha = 0.05$. The normal distribution of data was assessed using the Shapiro-Wilk test. Population data are presented as mean (±standard deviation). Pearson correlation analysis was conducted to test whether SW speed and dynamometry-based tensile stiffness were correlated at different levels of MVC loading.

3. Results

The average dimensions of all Achilles tendons that were imaged in this study are shown in Table 1. The average maximum MVC tendon strain was 6.1 % (±1.8 %) (Table 1). The average dynamometry-based stiffness at 10 % of maximum MVC strain was 623 MPa (±243 MPa) and increased to 805 MPa (±490 MPa) and 853 MPa (±600 MPa) at 40 % and 70 % of MVC respectively (Fig. 5). For the same participants, average SW speed was 11.4 m/s (±1.2 m/s) leading to an estimation of Young's modulus of 0.396 MPa (±0.081 MPa).

Pearson correlation analysis indicated that dynamometry-based stiffness was correlated to SW speed ($r(10) = 0.604$, $p = .038$) and SW-based Young's modulus ($r(10) = 0.620$, $p = .031$) only at 10 % of MVC elongation (moderate to good correlation (Overholser & Sowinski, 2008)). No significant correlation ($p > 0.05$) was found between SW-based and dynamometry-based measurements of stiffness for higher levels of loading (Fig. 6). Please refer to supplementary material for all correlation graphs.

4. Discussion

The main finding of the current study was that SW-based measurements of Achilles tendon stiffness were correlated to the gold-standard measurements of stiffness only for 10 % of MVC, which in turn corresponds to a tendon strain of 0.6 % (±0.2 %) (Table 1). No correlation (p

Table 1
Participants' Achilles tendon dimensions and dynamometry-based measurements. Measurements are presented as average (±standard deviation). (*) Values corrected for antagonist co-activation of tibialis anterior.

Thickness (cm)	0.48 (±0.04)
CSA (cm^2)	0.50 (±0.13)
Moment arm length (cm)	3.43 (±0.53)
Whole tendon length (cm)	22.0 (±3.2)
Free tendon length (cm)	6.2 (±1.5)
MVC maximum strain (%)	6.1 (±1.8)
*MVC maximum torque (Nm)	85 (±31)
*MVC maximum Force (N)	2530 (±876)
*MVC maximum stress (MPa)	53 (±21)

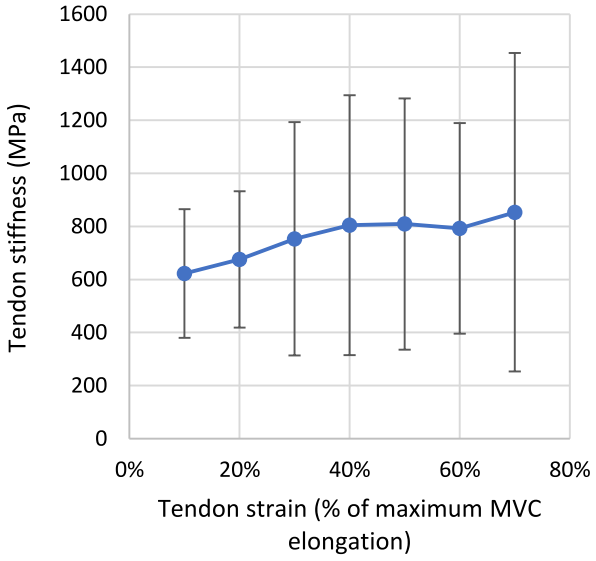

Fig. 5. Average dynamometry based measurements of tendon stiffness with increasing tendon strain. Stiffness is assessed as the slope of the stress–strain graph. Tendon strain is presented as (%) of maximum MVC elongation.

> 0.05) was found for higher levels of loading in the tendon. This observation indicates that supersonic SW elastography measurements are more likely to be relevant to tendon stiffness only for small strains (i.e., the initial slope of its stress–strain graph). To the authors' knowledge, the present study is the first to make this observation *in vivo*. This finding agrees with an *in vitro* study testing human cadaveric tendons (Haen et al., 2017), in which a significant correlation between SW-based stiffness of fresh frozen Achilles tendons and elastic modulus was found for small tendon elongations before a disruption point at a mean of 0.16 % (±0.11 %) strain.

A direct comparison between the absolute values of SW-based and dynamometry-based measurements revealed a substantial underestimation of Young's modulus by SW elastography. The observed substantial difference between methods should not come as a surprise considering the fact that none of the hypotheses that enable the use of equation 1 to calculate Young's modulus from SW speed are met; namely the fact that the Achilles tendon is not linearly elastic, it is not homogenous and it is not isotropic. Although the SW-based estimations of Young's modulus were about three orders of magnitude lower than dynamometry, it is important to point out that the values of SW speed and dynamometry-based Young's modulus measured here are in line with relevant literature (DeWall et al., 2014).

Overall, the findings of this study indicate that supersonic SW elastography should be used in applications where the detection of differences between participants or groups of participants or the detection of changes over time are important outcome measures. Such applications could include the diagnosis and study of tendon pathologies (e.g., injury, tendinopathy), the study of the effect of rehabilitation interventions and the exploration of the adaptations or maladaptations of tendon biomechanics in response to extrinsic or intrinsic factors. At the same time, the conceptual limitation of trying to describe the complex non-linear mechanical response of Achilles tendon with a single measurement/number means that SW elastography is not applicable in studies where the quantification of tendon stress–strain behaviour is needed.

In the present study, SW speed was measured with the ankle joint in 10° of plantarflexion with no tension applied to the tendon by the in-series muscles. This was necessary to minimise the risk of image saturation in supersonic SW elastography (DeWall et al., 2014). One could argue that measuring SW speed with the ankle joint positioned at

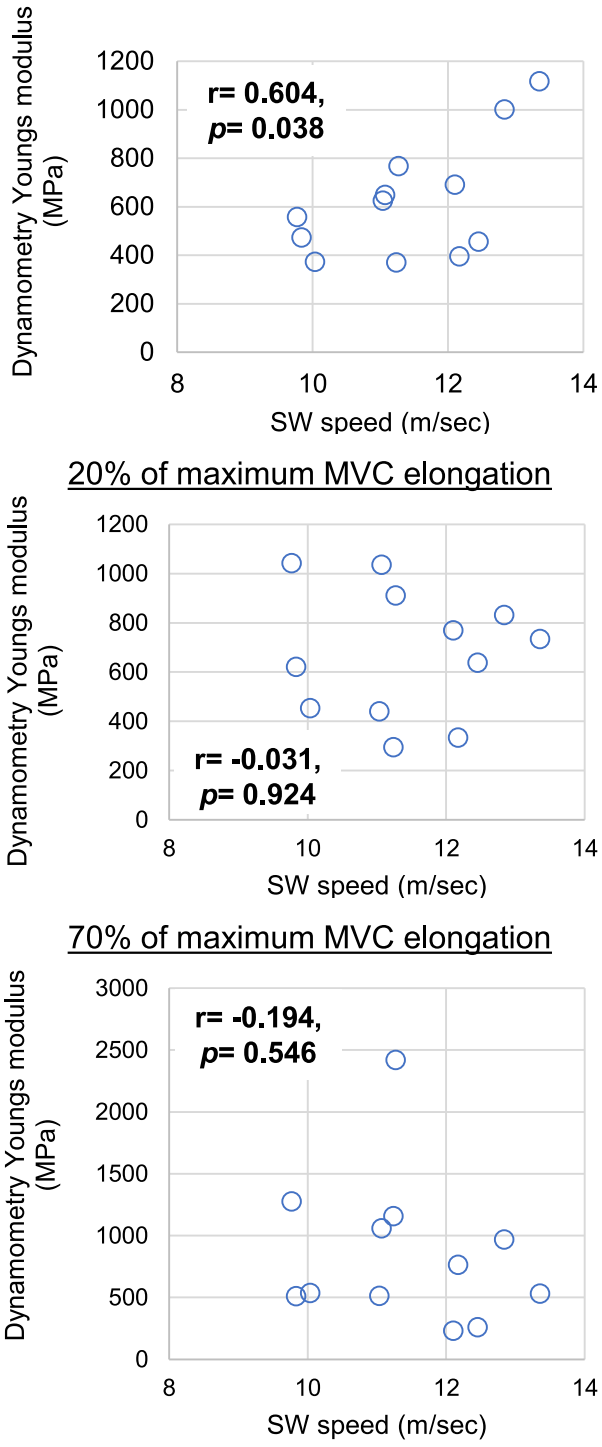

Fig. 6. Correlation between dynamometry-based and SW-based estimations of Achilles tendon Young's modulus for selected strain levels. Strain levels are presented as 10% increments of maximum MVC elongation. Strain levels of 10%, 20% and 70% of maximum MVC elongation are presented to demonstrate the loss of correlation beyond 10%. To this end, each graph is also accompanied by the respective r and *p* values of Pearson correlation analysis.

different angles and with increased levels of tension in the tendon would inevitably increase SW speed and the SW-based calculations of Young's modulus. However, it is unlikely that the comparative outcome of the two methods would have been affected substantially. Also, the three orders for magnitude difference was maintained even when the

comparison was against dynamometry-based stiffness for small strains (i.e., 10 % of MVC elongation). The same observation of three orders of magnitude difference was also made in the literature for continuous SW elastography (Corrigan et al., 2019). Continuous SW elastography is a different SW elastography modality which enables measuring SW speed in more functional positions such as ankle dorsiflexion without obtaining a saturated elastogram (Corrigan et al., 2019). At this point it should be noted that SW speed was measured only at the centre of the free tendon while dynamometry-based calculations of Young's modulus correspond to the entire Achilles tendon (medial path). The centre of the free tendon was chosen as the most appropriate site for SW elastography measurements based on literature indicating that SW speed is at its highest in the free tendon (DeWall et al., 2014).

In the present study, the gold-standard dynamometry method was used to assess tendon stress–strain behaviour for elongations up to 80 % of MVC. The analysis was restricted to the first 80 % of MVC because, for this part of the contraction, all participants were able to consistently generate a ramped increase in the generated torque. In many cases, the rate of increase in torque became erratic beyond this point. The slope of the stress–strain graph was then calculated based on curve fitting for a minimum of 10 % and a maximum of 70 % of MVC strain. Zero and 80 % were excluded from slope calculations to avoid errors due to poor curve fitting at the limits of available data. The inability of participants to generate a continuous ramped output of torque beyond ≈80 % of MVC could be caused by poor familiarisation with the task. This could also explain the low values of maximum tendon strain during MVC (Table 1). Additionally, in the present study the ramp contraction was initiated with the foot in a neutral position, which may be associated with some pre-loading of the tendon (Muramatsu et al., 2001).

Last but not least, the dynamometry-based results presented here are likely to be affected by potential movement of the heel during MVC. More specifically, our inherent inability to rigidly fix the ankle during *in vivo* testing can affect the accuracy of the measured ankle joint moments. Although extra care was taken to reduce potential heel movement during MVC with the use of added supports, it is established in the literature that the risk for relative heel movement cannot be fully eliminated (Arampatzis et al., 2005).

5. Conclusions

Measurements of SW speed from supersonic SW elastography enable the detection and study of differences and changes in tendon biomechanics, but the present *in vivo* application on the human Achilles tendon shows that the absolute values of the predicted Young's modulus are not accurate.

Most importantly, changes or differences in SW speed measured from supersonic SW elastography reflect changes/ differences in tendon stiffness corresponding to small strains. Supersonic SW elastography, in its current form, does not appear to be capable of offering any information about tendon biomechanics under load-bearing conditions. This limitation is unlikely to affect the value of supersonic SW elastography for the diagnosis and study of tendon pathologies and rehabilitation, as for these applications scanning is performed at rest. The above characteristics of supersonic SW elastography need to be taken into consideration on a study-specific basis to decide the appropriateness of the method and to inform the correct interpretation of results.

Ethics approval and consent to participate – Ethical approval from University of Staffordshire and each participant signed a consent form.

CRediT authorship contribution statement

Tiziana Mifsud: Conceptualization, Data curation, Formal analysis, Writing – original draft. **Panagiotis Chatzistergos:** Conceptualization, Data curation, Formal analysis, Validation, Writing – original draft. **Constantinos Maganaris:** Conceptualization, Validation, Writing – review & editing. **Nachiappan Chockalingam:** Conceptualization, Supervision, Writing – review & editing. **Nat Padhiar:** Supervision, Writing – review & editing. **Kirill Micallef Stafrace:** Writing – review & editing. **Alfred Gatt:** Supervision, Writing – review & editing.

Declaration of Competing Interest

The authors declare that they have no known competing financial interests or personal relationships that could have appeared to influence the work reported in this paper.

Acknowledgement & Funding

The primary author (TM) is a recipient of the Malta Sport Scholarship, financed by the Government of Malta.

Appendix A. Supplementary material

Supplementary data to this article can be found online at https://doi.org/10.1016/j.jbiomech.2023.111558.

Reference

Arampatzis, A., Stafilidis, S., DeMonte, G., Karamanidis, K., Morey-Klapsing, G., Brüggemann, G.P., 2005. Strain and elongation of the human gastrocnemius tendon and aponeurosis during maximal plantarflexion effort. J. Biomech. 38 (4), 833–841.
Bercoff, J., Tanter, M., Fink, M., 2004. Supersonic shear imaging: a new technique for soft tissue elasticity mapping. IEEE Trans. Ultrason. Ferroelectr. Freq. Control 51 (4), 396–409.
Bjornaraa, J., Di Fabio, R.P., 2011. Knee kinematics following ACL reconstruction in females; the effect of vision on performance during a cutting task. Int. J. Sports Phys. Ther. 6 (4), 271.
Bojsen-Møller, J., Hansen, P., Aagaard, P., Svantesson, U., Kjaer, M., Magnusson, S.P., 2004. Differential displacement of the human soleus and medial gastrocnemius aponeuroses during isometric plantar flexor contractions in vivo. J. Appl. Physiol. 97 (5), 1908–1914.
Botar-Jid, C.M., Cosgarea, R., Bolboacă, S.D., Şenilă, S.C., Lenghel, L.M., Rogojan, L., Dudea, S.M., 2016. Assessment of cutaneous melanoma by use of very-high-frequency ultrasound and real-time elastography. Am. J. Roentgenol. 206 (4), 699–704.
Chatzistergos, P.E., Behforootan, S., Allan, D., Naemi, R., Chockalingam, N., 2018. Shear wave elastography can assess the in-vivo nonlinear mechanical behavior of heel-pad. J. Biomech. 80, 144–150.
Chatzistergos, P.E., Chockalingam, N., 2022. An in vivo model for overloading-induced soft tissue injury. Sci. Rep. 12 (1), 1–10.
Chiu, T.R., Ngo, H., Lau, L., Leung, K., Lo, M., Yu, H., Ying, M., 2016. An investigation of the immediate effect of static stretching on the morphology and stiffness of achilles tendon in dominant and non-dominant legs. PLoS One 11 (4), e0154443.
Corrigan, P., Zellers, J.A., Balascio, P., Silbernagel, K.G., Cortes, D.H., 2019. Quantification of mechanical properties in healthy Achilles tendon using continuous shear wave elastography: a reliability and validation study. Ultrasound Med. Biol. 45 (7), 1574–1585.
Crawford, S.K., Thelen, D., Yakey, J.M., Heiderscheit, B.C., Wilson, J.J., Lee, K.S., 2022. Regional shear wave elastography of Achilles tendinopathy in symptomatic versus contralateral Achilles tendons. Eur. Radiol. 1–10.
De Luca, C.J., Gilmore, L.D., Kuznetsov, M., Roy, S.H., 2010. Filtering the surface EMG signal: Movement artifact and baseline noise contamination. J. Biomech. 43 (8), 1573–1579.
DeWall, R.J., Slane, L.C., Lee, K.S., Thelen, D.G., 2014. Spatial variations in Achilles tendon shear wave speed. J. Biomech. 47 (11), 2685–2692.
Dirrichs, T., Quack, V., Gatz, M., Tingart, M., Kuhl, C.K., Schrading, S., 2016. Shear wave elastography (SWE) for the evaluation of patients with tendinopathies. Acad. Radiol. 23 (10), 1204–1213.
Gatt, A., Chockalingam, N., Chatzistergos, P., Gatt, R., Schembri-Wismayer, P., Grima, J. N., Formosa, C., 2021. The biomechanical properties of human fresh-frozen vs thiel embalmed foot tendons.
Haen, T., Roux, A., Soubeyrand, M., Laporte, S., 2017. Shear waves elastography for assessment of human Achilles tendon's biomechanical properties: an experimental study. J. Mech. Behav. Biomed. Mater. 69, 178–184.
Hermens, H.J., Freriks, B., Merletti, R., Stegeman, D., Blok, J., Rau, G., Disselhorst-Klug, C., Hägg, G., 1999. European recommendations for surface electromyography. Roessingh Res. Dev. 8 (2), 13–54.
Liao, X., Kemp, S., Corner, G., Eisma, R., Huang, Z., 2015. Elastic properties of Thiel-embalmed human ankle tendon and ligament. Clin. Anat. 28 (7), 917–924.
Maganaris, C.N., 2003. Tendon conditioning: artefact or property? Proceedings of the Royal Society of London. Series B: Biological Sciences 270 (suppl_1), S39–S42.
Maganaris, C.N., 2004. Imaging-based estimates of moment arm length in intact human muscle-tendons. Eur. J. Appl. Physiol. 91 (2), 130–139.

Maganaris, C.N., 2005. Validity of procedures involved in ultrasound-based measurement of human plantarflexor tendon elongation on contraction. J. Biomech. 38 (1), 9–13.
Maganaris, C.N., Paul, J.P., 1999. In vivo human tendon mechanical properties. J. Physiol. 1 (521), 307–331.
Maganaris, C.N., Baltzopoulos, V., Sargeant, A.J., 1998. Differences in human antagonistic ankle dorsiflexor coactivation between legs; can they explain the moment deficit in the weaker plantarflexor leg? Exp. Physiol. 83 (6), 843–855.
Maganaris, C.N., Chatzistergos, P., Reeves, N.D., Narici, M.V., 2017. Quantification of internal stress-strain fields in human tendon: unraveling the mechanisms that underlie regional tendon adaptations and mal-adaptations to mechanical loading and the effectiveness of therapeutic eccentric exercise. Front. Physiol. 8, 91.
Merletti, R., 2000. Surface electromyography: The SENIAM project. Eur. J. Phys. Rehabil. Med. 36 (4), 167.
Morgan, G.E., Martin, R., Williams, L., Pearce, O., Morris, K., 2018. Objective assessment of stiffness in Achilles tendinopathy: a novel approach using the MyotonPRO. BMJ Open Sport Exerc. Med. 4 (1), e000446.
Muramatsu, T., Muraoka, T., Takeshita, D., Kawakami, Y., Hirano, Y., Fukunaga, T., 2001. Mechanical properties of tendon and aponeurosis of human gastrocnemius muscle in vivo. J. Appl. Physiol. 90 (5), 1671–1678.
Overholser, B.R., Sowinski, K.M., 2008. Biostatistics primer: part 2. Nutr. Clin. Pract. 23 (1), 76–84.
Payne, C., Watt, P., Cercignani, M., Webborn, N., 2018a. Reproducibility of shear wave elastography measuresof the Achilles tendon. Skeletal Radiol. 47 (6), 779–784.
Payne, C., Watt, P., Webborn, N., 2018b. Shear wave elastography measures of the Achilles Tendon: Influence of time of day, leg dominance and the impact of an acute 30-minute bout of running. Appl. Sci. 8 (7), 1170.
Sarvazyan, A.P., Urban, M.W., Greenleaf, J.F., 2013. Acoustic waves in medical imaging and diagnostics. Ultrasound Med. Biol. 39 (7), 1133–1146.
Scholz, M.N., Bobbert, M.F., Van Soest, A.J., Clark, J.R., van Heerden, J., 2008. Running biomechanics: shorter heels, better economy. J. Exp. Biol. 211 (20), 3266–3271.
Slane, L.C., Martin, J., DeWall, R., Thelen, D., Lee, K., 2017. Quantitative ultrasound mapping of regional variations in shear wave speeds of the aging Achilles tendon. Eur. Radiol. 27 (2), 474–482.
Slane, L.C., Thelen, D.G., 2015. Achilles tendon displacement patterns during passive stretch and eccentric loading are altered in middle-aged adults. Med. Eng. Phys. 37 (7), 712–716.
Stenroth, L., Cronin, N.J., Peltonen, J., Korhonen, M.T., Sipilä, S., Finni, T., 2016. Triceps surae muscle-tendon properties in older endurance-and sprint-trained athletes. J. Appl. Physiol. 120 (1), 63–69.
Verstraete, M.A., Van Der Straeten, C., De Lepeleere, B., Opsomer, G., Van Hoof, T., Victor, J., 2015. Impact of drying and thiel embalming on mechanical properties of achilles tendons. Clin. Anat. 28 (8), 994–1001.
Widman, E., Maksuti, E., Larsson, D., Urban, M.W., Bjällmark, A., Larsson, M., 2015. Shear wave elastography plaque characterization with mechanical testing validation: a phantom study. Phys. Med. Biol. 60 (8), 3151.
Zhao, H., Ren, Y., Wu, Y., Liu, S.Q., Zhang, L., 2009. Ultrasonic evaluations of Achilles tendon mechanical properties poststroke. J. Appl. Physiol. 106 (3), 843–849.